

Feedback System for Energy and Beam Position Stabilization.

Valeri Lebedev

1. The results of the beam motion study

The study of the beam motion at different places of the accelerator has shown that the beam has the excursions in energy and in both transverse planes. Currently, we have many measurements of the beam motion but the measurement results performed at ARC1 (January 96) and Hall C line (October 1996) will be mainly discussed because they exhibit the main characteristics of the beam motion with good resolution and, consequently, their results determine the requirements to the feedback system.

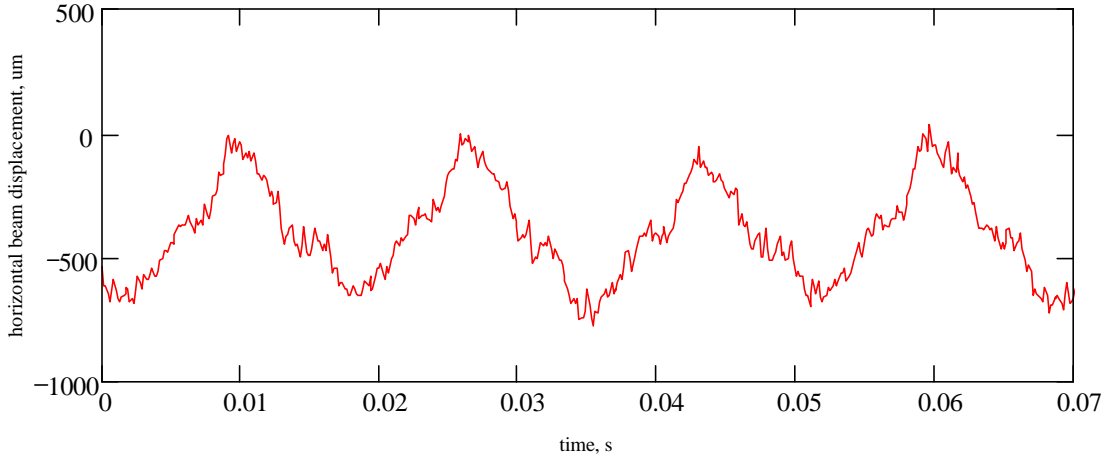
The spectral density of the beam motion can be separated in two main parts: the low frequency part with frequency below 60 Hz and high frequency part due to beam motion at frequencies of power line harmonics.

The measurement in ARC1 were performed January 21, 1996 with SEE BPMs at sampling rate of 113.7 kHz and duration of one measurement of 0.144 s. They showed that for time less than 1 s the power line harmonics make the main contribution into beam motion. The amplitude of beam displacement was about 100 μm at 60 Hz and 30 μm at 180 Hz. The amplitude of relative energy oscillations was about $3 \cdot 10^{-5}$ at 60 Hz and $2 \cdot 10^{-5}$ at 180 Hz. In a few of these measurements there were peaks at 120 Hz and 240 Hz but their values were significantly smaller. A contribution from other power line harmonics was not observed. They demonstrated that for the beam current of about 10 μA the rms accuracy of the BPMs related to the electronic noise was 40-50 μm .

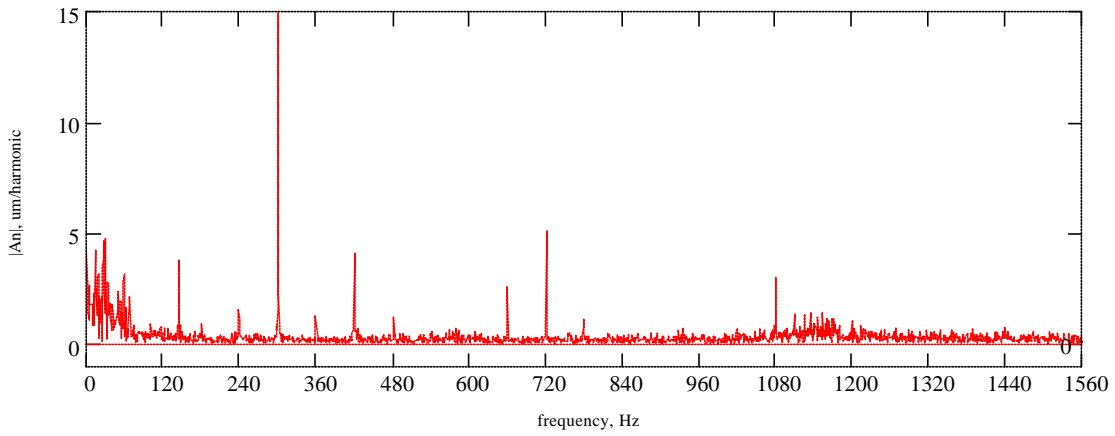
The measurement in the Hall C line was performed in October 24, 1996, with the transport line SEE BPMs at sampling rate of 7141 kHz. The transport line SEE BPMs have longer integration time and therefore better accuracy. Their measurement time is 16 times longer and, consequently, the spectrum of the beam motion can be obtained for 16 times smaller frequency. From this point of view this data is more valuable for the feedback system design. There are 5 sets of data measured during 6 s.

Figure 1a shows an example of measured data. To obtain a better resolution for the beam motion spectrum the first three power line harmonics were subtracted from the measurements before performing the FFT. Their amplitudes and phases were fitted by the least square root method and shown in Tables 1 and 2. Figure 1b exhibits the spectrum of the signal shown in Figure 1a without the first three harmonics in it. One can observe many power line harmonics which spread up to 1.2 kHz. Most powerful harmonics are at 300 and 720 Hz. The noisy plateau in the spectrum is related to the noise of BPM electronics and determines the rms BPM resolution of about 20 μm for beam current of 38 μA which is in a reasonable agreement with the laboratory measurements.

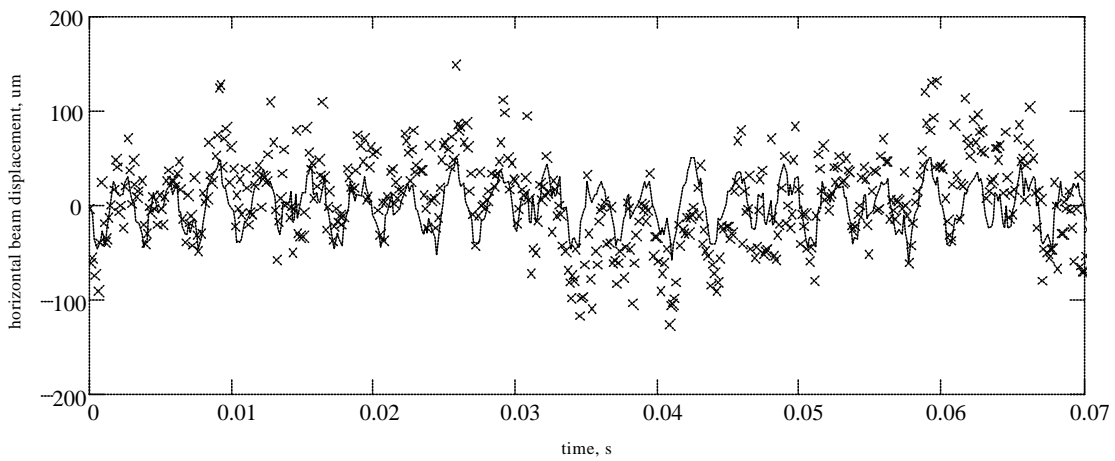
The residual value of beam motion in BPM signal after subtraction of these first harmonics is comparable with BPM noise. Thus, to estimate the beam displacement due to the rest of the power line harmonics one needs to separate noise of BPM electronics from the real beam signal. The spectral density of the BPM noise does not depend on frequency and we can reasonably guess that noise plateau in the signal is totally related to the BPM noise. Therefore the signal spectrum was filtered so that only the harmonics near the power line frequencies were left. Then the inverse FFT produces a signal which characterizes the beam motion at higher power line harmonics. Figure 1c shows signals for the case when the first three harmonics are subtracted from the signal. Here the crosses show the BPM signal and the solid line shows an estimate of beam motion related due to power line harmonics (without the first three harmonic).



a)



b)



c)

Figure 1. Beam motion at IPM3C12: a) measured signal (only first 70 ms are shown), b) spectrum without first three harmonics, c) measured signal without first three harmonics - \times , and an estimate of the beam displacement due to higher power line harmonics - solid line. Beam current is equal to $38 \mu\text{A}$, and the beam energy is 3.245 GeV.

Low frequency part of the signal spectrum presented in Figure 1 are shown in Figure 2. One can see that it spreads from 0 to about 70 Hz and does not have definite frequencies. Frequencies of about 30 and 58 Hz make the largest contribution. Earlier in the measurements in the ARC2 we observed large phase oscillations of 60 Hz beam motion. The frequency of these oscillations was about 1 Hz and they are apparently related to this 58 Hz component. There is also peak at 145 Hz frequency which origination is unknown.

The energy oscillation which can be estimated from Hall C measurements is about 2 times larger than measured at ARC1 and are equal to $6 \cdot 10^{-5}$ at 60 Hz and $2 \cdot 10^{-5}$ at 180 Hz.

Table 1. Amplitudes of power line harmonic at IPM3C12 for different measurements

File name	long11	long21	long31	long41	long51
Amplitude at 60 Hz, μm	236.9	255.8	240.9	230.9	266.9
Amplitude at 120 Hz, μm	24.8	25.5	22.9	22.1	22.1
Amplitude at 180 Hz, μm	54.7	54.2	54.5	55.6	53.4
Residual rms beam motion at other power line harmonics, μm	25.9	25.2	24.7	25.8	26.05

Table 2. Amplitudes of power line harmonic at different BPMs (file: long11)

BPM name	IPM3C07		IPM3C08		IPM3C12	
	x	y	x	y	x	y
Amplitude at 60 Hz, μm	100.3	198.7	109.6	111.2	236.9	44.3
Amplitude at 120 Hz, μm	12.9	47.5	13.8	25.7	24.8	6.21
Amplitude at 180 Hz, μm	18.5	123.1	13.9	64.1	54.7	5.1
Residual rms beam motion at other power line harmonics, μm	10.8	47.9	8.8	26.1	25.2	6.7

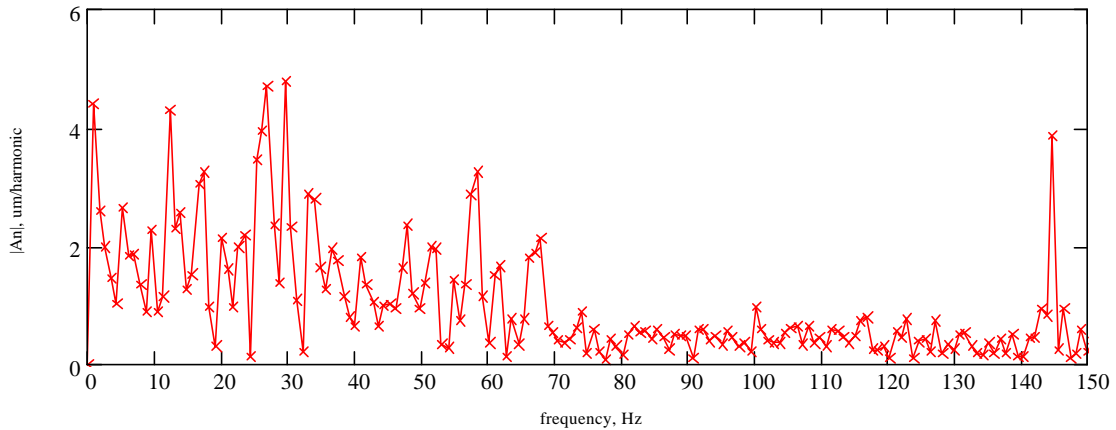


Figure 2. Low frequency part of the spectrum presented in Figure 1.

2. The beam motion and general requirements to the feedback system

The requirements to the beam position and energy stabilization are determined by the natural beam energy spread and size on the target which allows to reach the highest beam quality. Table 2 exhibits the main parameters of 4 GeV beam and main requirements to the feedback system. The level of stabilization was chosen so that the feedback system contribution should not exceed 20% for the beam size and 10% for the energy spread. The safety margin of about 10 dB was put into the suppression values to anticipate a

possible enlargement of beam motion at a long machine run. We use here the effective beam emittance (Courant-Snyder invariant)

$$e = bq^2 + 2aqx + gx^2, \quad (1)$$

to describe the requirements to the transverse beam motion independently on the machine beta-functions. Here b is the design beta-function, $2a = -db/dz$ and $g = (1+a^2)/b$, x and q are the beam displacement and angle at the exit of the feedback system. It is important to note that the level of intrinsic noise of the feedback system due to noise of the BPM measurements is an important issue of feedback system design. The last part of the table shows requirements to the beam motion due to feedback system noise.

Table 2. Main parameters of the beam and requirements

Natural beam parameters (sizes without beam motion)	
Beam emittance at 4.045 GeV, rms	0.06 nm
Relative beam energy spread, rms	15 ppm
Requirements to beam motion at the feedback exit	
Effective beam emittance, rms	< 0.024 nm
Relative energy spread, rms	< 6.7 ppm
Requirements to suppression at different frequencies	
Suppression of 60, 120, 180 and 240 Hz	< 30 db
Suppression at frequency of 30 Hz	< 20 db
Suppression at frequency less 30 Hz	< {600/f[Hz]} db
Requirements to the beam motion excited by the feedback system itself	
Effective emittance excited by feedback system noise, rms	< 0.015 nm
Relative energy fluctuations excited by feedback system noise, rms	< 5 ppm

The current status of the CEBAF accelerator is sufficiently good, so that the energy and position oscillations do not limit machine operation and do not cause any significant decrease of the free aperture. Thus, it is sufficient to use only one feedback system (for each hall) to get the required by physics experiments improvement of the beam stability. Such systems has to be located in each hall and have to stabilize the beam position in a corresponding hall transport line. One hall only can be chosen for the energy stabilization. It implies that if there is another hall utilizing the same energy it will get the same good energy stabilization. In the case of another energy the energy stabilization can be spoiled by energy fluctuations in injector and by phase fluctuations of the accelerating voltage of main linacs. The first can be fixed by the injector feedback system while the second can be improved by careful path-length adjustments for multipass operation. Below we will consider one system which can be located in any of two Halls (Hall A or Hall C) taking into account that they have similar optics and use the same kind of hardware.

2. Optics and BPM resolution.

The optics for Halls A and C was recently changed to increase the horizontal dispersion and get optimal conditions for beam position stabilization. The beta-functions, dispersion and betatron phase advances for Hall C are shown in Figure 3 (Hall A have a close optics). One can see that the peak dispersion was increased in about two times in comparison with base line design. There are also larger beta-functions; and the betatron phase advances between corresponding BPMs are about 90° what is optimal for the feedback system space resolution. The list of BPMs and correctors for the feedback system is shown in Table 3. The design beta-functions, dispersion and phase advances are also shown in the table.

First we consider an accuracy of the extraction of vertical beam position and angle from the BPM measurements. Taking into account that the position and angle of the beam are changed during beam transportation we will use the Courant-Snyder invariant (effective emittance of beam transverse motion) to express the accuracy of the beam position measurements.

Table 3.

NAME	BetaX	AlfaX	BetaY	AlfaY	DspX	DspXp	NuX	NuY
MHC3C02V	1384.96	-1.43703	7369.51	12.0956	-26.251	-0.0422399	0.174094	0.162417
MHC3C04H	1540.29	1.55229	984.911	-2.16622	0	0	0.552712	0.332461
MHC3C07V	1782.47	-1.97754	2980.6	2.52495	0	0	0.727567	0.45876
IPM3C07V	1782.47	-1.97754	2980.6	2.52495	0	0	0.727567	0.45876
MHC3C08H	5006.89	3.45412	856.768	-0.16704	0	0	0.759623	0.522437
IPM3C08H	5006.89	3.45412	856.768	-0.16704	0	0	0.759623	0.522437
IPM3C11V	533.17	-1.22738	3960.65	3.13558	-178.288	-0.439734	1.04742	0.675235
IPM3C12H	2863.36	3.5097	1528.95	-1.91525	-411.104	0.497332	1.11394	0.710287
IPM3C16H	5107.75	2.39168	1684.61	-1.58651	0.00273287	-9.17184e-06	1.4764	0.843045

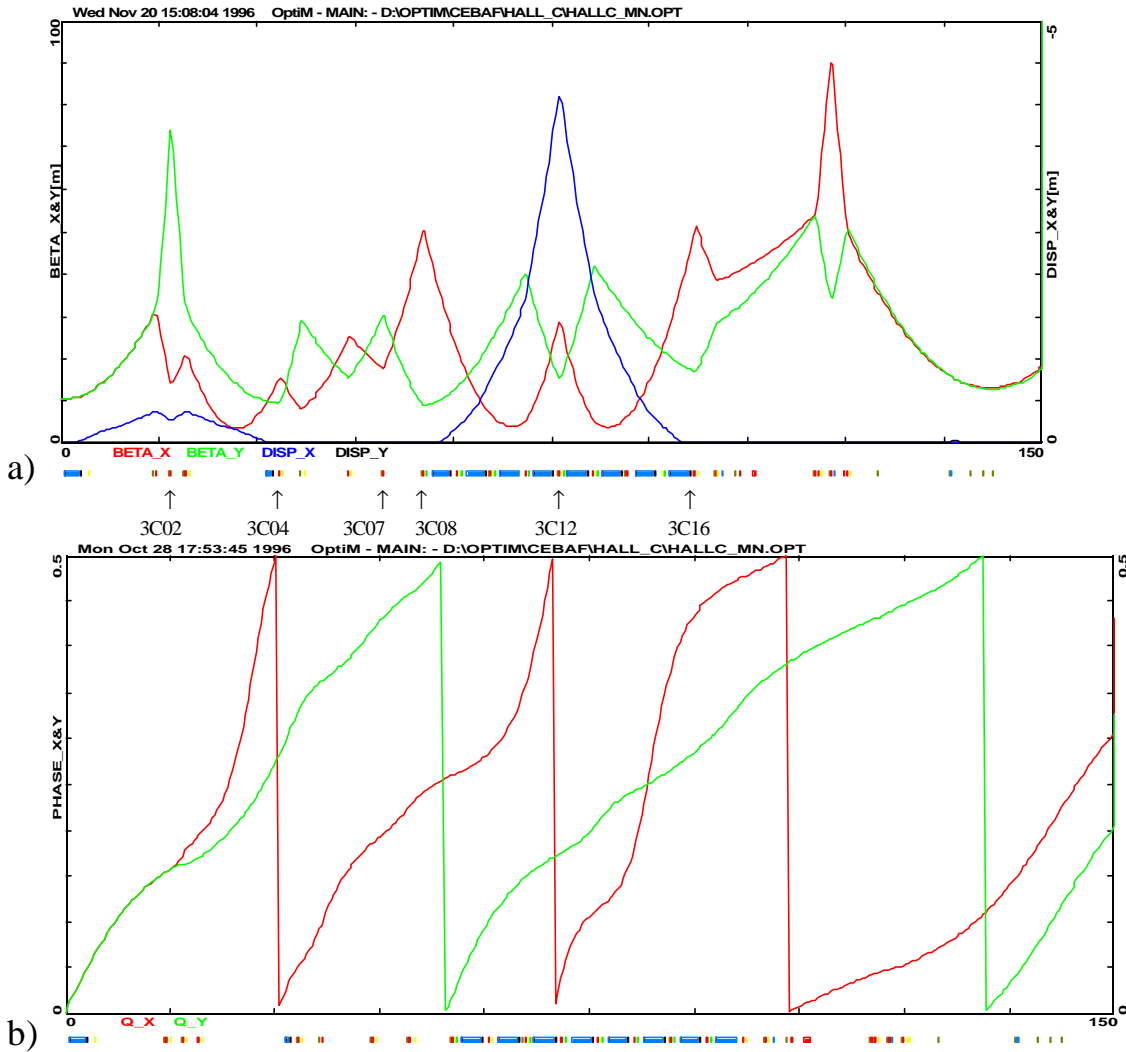


Figure 3. Beta-functions and dispersion a) and betatron phase advances b) for Hall C transport line.

Let \mathbf{M} be the transfer matrix for vertical motion between two BPMs. Then we can write that the position and angle at BPM2, y_2 and \mathbf{q}_{y2} , are bound with the position and angle at BPM1, y_1 and \mathbf{q}_{y1} , by the following equation

$$\begin{aligned}
\begin{vmatrix} y_2 \\ \mathbf{q}_{y2} \end{vmatrix} &= \mathbf{M} \begin{vmatrix} y_1 \\ \mathbf{q}_{y1} \end{vmatrix} = \begin{vmatrix} M_{33} & M_{34} \\ M_{43} & M_{44} \end{vmatrix} \begin{vmatrix} y_1 \\ \mathbf{q}_{y1} \end{vmatrix} = \\
&= \sqrt{\frac{\mathbf{b}_{y2}}{\mathbf{b}_{y1}}} \begin{vmatrix} \cos \mathbf{m}_y + \mathbf{a}_{y1} \sin \mathbf{m}_y & \mathbf{b}_{y1} \sin \mathbf{m}_y \\ \frac{\mathbf{a}_{y1} - \mathbf{a}_{y2}}{\mathbf{b}_{y2}} \cos \mathbf{m}_y - \frac{\sin \mathbf{m}_y}{\mathbf{b}_{y2}} (1 + \mathbf{a}_{y1} \mathbf{a}_{y2}) & \frac{\mathbf{b}_{y1}}{\mathbf{b}_{y2}} (\cos \mathbf{m}_y - \mathbf{a}_{y2} \sin \mathbf{m}_y) \end{vmatrix} \begin{vmatrix} y_1 \\ \mathbf{q}_{y1} \end{vmatrix}, \quad (2)
\end{aligned}$$

where \mathbf{b}_{y1} , \mathbf{b}_{y2} , \mathbf{a}_{y1} and \mathbf{a}_{y2} are beta-functions and their negative half-derivatives at BPMs 1 and 2, \mathbf{m}_y is the betatron phase advance between BPMs 1 and 2. Expressing \mathbf{q}_{y1} through y_2 and y_2 from Eq.(2) we obtain

$$\mathbf{q}_{y1} = \frac{y_2 - M_{33}x_1}{M_{34}}, \quad (3)$$

Substituting Eq.(3) into Eq.(1) we express the effective beam emittance through BPM measurements

$$\mathbf{e}_y = \mathbf{b}_{y1} \left(\frac{y_2 - M_{33}y_1}{M_{34}} \right)^2 + 2\mathbf{a}_{y1} \left(\frac{y_2 - M_{33}y_1}{M_{34}} \right) y + \mathbf{g}_{y1}^2. \quad (4)$$

Taking into account that the noises of different BPMs are not correlated and are equal for both BPMs, $\overline{y_1^2} = \overline{y_2^2} = x_{BPM}^2$, and substituting matrix elements in Eq.(4) we finally obtain

$$\overline{\mathbf{e}_y} = \left(\frac{1}{\mathbf{b}_{y1}} + \frac{1}{\mathbf{b}_{y2}} \right) \frac{x_{BPM}^2}{\sin^2 \mathbf{m}_y} \quad (5)$$

Substituting the beta-functions and the betatron phase advance from Table 3 we obtain EMBED Equation.2 **Error! Objects cannot be created from editing field codes.** =0.024 nm for xBPM = 20 mm.

Now we consider an accuracy of the extraction of energy, beam position and angle from BPM measurements. The beam displacements due to energy change and due to horizontal betatron motion are coupled at IPM3C12 due to non zero dispersion at its location. To simplify calculations we will use an approach different from considered above. Expressing beam displacement through effective emittance, and momentum error we can write down where m is the betatron phase advance \mathbf{b}_{x1} , \mathbf{b}_{x2} and \mathbf{b}_{x3} are the beta-functions at corresponding BPMs, m_1 and m_2 are the betatron phase advances between BPM1 and other two BPMs, and,

Performing matrix inversion, $\mathbf{N} = \mathbf{M}^{-1}$, and taking into account that $D_1 = D_3 = 0$ we obtain

$$\begin{aligned}
\begin{vmatrix} X \\ P \\ \Delta p / p \end{vmatrix} &= \mathbf{N} \begin{vmatrix} x_1 \\ x_2 \\ x_3 \end{vmatrix} = \begin{vmatrix} N_{11} & N_{12} & N_{13} \\ N_{21} & N_{22} & N_{23} \\ N_{31} & N_{32} & N_{33} \end{vmatrix} \begin{vmatrix} x_1 \\ x_2 \\ x_3 \end{vmatrix} = \\
&= \frac{1}{\sqrt{\mathbf{b}_{x1} \mathbf{b}_{x3} D_2 \sin \mathbf{m}_2}} \cdot \begin{vmatrix} \sqrt{\mathbf{b}_{x3}} D_2 \sin \mathbf{m}_2 & 0 & 0 \\ -\sqrt{\mathbf{b}_{x3}} D_2 \cos \mathbf{m}_2 & 0 & \sqrt{\mathbf{b}_{x1}} D_2 \\ -\sqrt{\mathbf{b}_{x2} \mathbf{b}_{x3}} \sin(\mathbf{m}_1 + \mathbf{m}_2) & \sqrt{\mathbf{b}_{x1} \mathbf{b}_{x3}} \sin \mathbf{m}_2 & \sqrt{\mathbf{b}_{x1} \mathbf{b}_{x2}} \sin \mathbf{m}_1 \end{vmatrix} \begin{vmatrix} x_1 \\ x_2 \\ x_3 \end{vmatrix}. \quad (8)
\end{aligned}$$

The same as for vertical motion we take into account that the noises of different BPMs are not correlated and are equal for all three BPMs, $\overline{x_1^2} = \overline{x_2^2} = \overline{x_3^2} = x_{BPM}^2$. Performing averaging we obtain expressions for the accuracy of the energy measurement,

$$\begin{aligned} \frac{\sqrt{\Delta p^2}}{p} &= \sqrt{(N_{31}^2 + N_{32}^2 + N_{33}^2)x_{BPM}^2} = \\ &= \frac{x_{BPM}}{D_2} \sqrt{1 + \frac{\mathbf{b}_2}{\sin^2(\mathbf{m}_2)} \left(\frac{\sin^2(\mathbf{m}_1 + \mathbf{m}_2)}{\mathbf{b}_1} + \frac{\sin^2(\mathbf{m}_1)}{\mathbf{b}_3} \right)}, \end{aligned} \quad (9)$$

and for the accuracy of the effective emittance measurement,

$$\begin{aligned} \overline{\mathbf{e}_x} &= \overline{X^2 + P^2} = (N_{11}^2 + N_{12}^2 + N_{13}^2 + N_{21}^2 + N_{22}^2 + N_{23}^2)x_{BPM}^2 = \\ &= \left(\frac{1}{\mathbf{b}_{x1}} + \frac{1}{\mathbf{b}_{x3}} \right) \frac{x_{BPM}^2}{\sin^2 \mathbf{m}_2}. \end{aligned} \quad (10)$$

As one has to expect for the case of zero dispersion at BPMs 1 and 3 Eq.(10) is similar to Eq.(5) for the vertical motion. Substituting the beta-functions, the dispersion and the betatron phase advances from Table 3 we obtain $\overline{\mathbf{e}_x} = 0.017$ nm and $\sqrt{\Delta p^2} / p = 5.9 \cdot 10^{-6}$ for $x_{BPM} = 20$ μm . As follows from Eqs.(9) and (10) the optics is close to be totally optimized: $\sin^2 \mu_2 = 0.957$ (desired value - 1.0), $\sin^2(\mu_1 + \mu_2) = 0.187$ (desired value - 0.0), $\sin^2 \mu_1 = 0.629$ (desired value - 0.0), $\mathbf{b}_2/\mathbf{b}_1 \approx \mathbf{b}_2/\mathbf{b}_3 \approx 0.56$ (desired value $\mathbf{b}_2/\mathbf{b}_1, \mathbf{b}_2/\mathbf{b}_3 \ll 1$); that results that a loss in energy resolution is about 20% ($\sqrt{\Delta p^2} / p \approx 1.22 x_{BPM}/D_2$).

Thus, we can conclude that to reach the required level of stabilization we need the effective BPM resolution better than 20 μm .

3. Frequency response of the feedback system

For simplicity we will consider at the beginning the frequency response of scalar system (one input - one output). As can be shown later this consideration can be easily generalized for the case of the considered feedback system. The scheme of the system is shown in Figure 4. The feedback system measures the error on its output $y(t)$ and corrects its input signal $x(t)$ so that they are related by following equation

$$y(t) = x(t) + c(t), \quad (11)$$

where $c(t)$ is the value of the correction. The measurement of the system output signal are performed with errors Δy_n .

We will neglect delays in the system and we can write in frequency domain

$$\begin{aligned} x_n &\equiv x(t_n) = x_w e^{i\omega t_n} \\ y_n &\equiv y(t_n) = y_w e^{i\omega t_n}, \quad t_n = Tn, \\ c_n &\equiv c(t_n) = c_w e^{i\omega t_n} \end{aligned} \quad (12)$$

where T is the sampling time. Let us denote the system transfer function in frequency domain

$$K(\omega) = \frac{y_w}{x_w}, \quad (13)$$

and the system amplification

$$G(\omega) = \frac{c_w}{y_w}. \quad (14)$$

Then performing Fourier transform for Eq.(11),

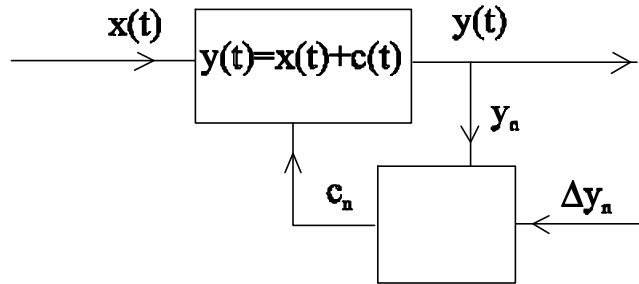


Figure 4. Scheme of the scalar feedback system.

$$y_w = x_w + c_w \quad , \quad (15)$$

and using Eqs.(13) and (14) we obtain

$$K(\mathbf{w}) = \frac{1}{1 - G(\mathbf{w})} \quad . \quad (16)$$

To determine the effect of BPM noise on the feedback system we will consider the system with zero signal on its input. Then using Eqs.(14) and (15) we can write that output signal is

$$y_w = G(\mathbf{w})(y_w + \Delta y_w) \quad , \quad (17)$$

where we took into account that the measured signal is $y_w + \Delta y_w$. Solving this equation relative to y_w and substituting $G(\mathbf{w})$ from Eq.(16) we obtain

$$y_w = (K(\mathbf{w}) - 1)\Delta y_w \quad . \quad (18)$$

The spectral density of the noise does not depend of frequency and on frequency interval $\mathbf{w}\hat{\mathbf{I}}[0, \pi/T]$ is equal to

$$\overline{\Delta y_w^2} = \frac{T}{\mathbf{p}} \overline{\Delta y^2} \quad . \quad (19)$$

where $\sqrt{\overline{\Delta y^2}}$ is the rms error of the measurement. Then the spectral density of noise on the system output is equal to

$$\overline{y_w^2} = \frac{T}{\mathbf{p}} |K(\mathbf{w}) - 1|^2 \overline{\Delta y^2} \quad . \quad (20)$$

That determines the rms error at the system output to be equal to

$$\overline{y^2} = \overline{\Delta y^2} \frac{T}{\mathbf{p}} \int_0^{p/T} |K(\mathbf{w}) - 1|^2 d\mathbf{w} \quad . \quad (21)$$

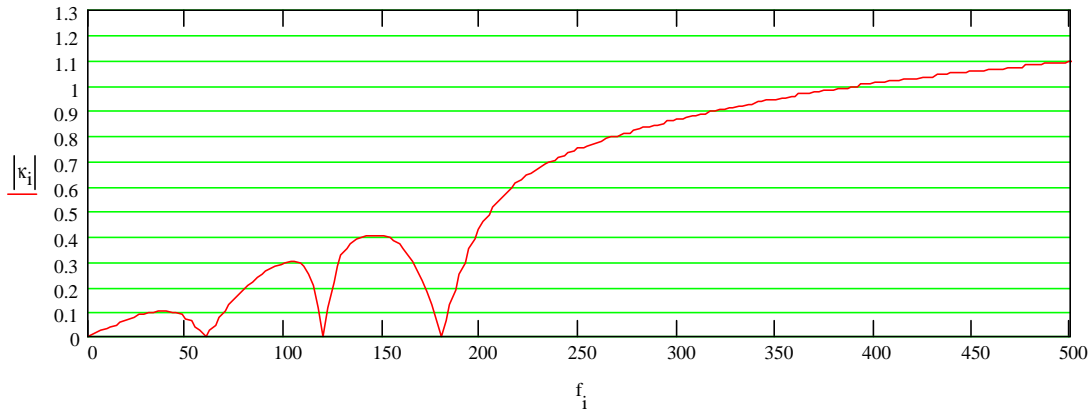
One can see that if $K(\mathbf{w})=1$ then the measurement noise does not affect the system output but at the same time the feedback system does not suppress the input signal. Thus, we can conclude that to minimize the effect of noise measurements one needs to design the system so that $K(\mathbf{w})$ would be close to one at frequencies where spectral density of the input signal $x(t)$ is sufficiently small.

As an example of such a system we consider the system with recursive digital filters at zero frequency and the first three power line harmonics. We will choose its transfer function as follows

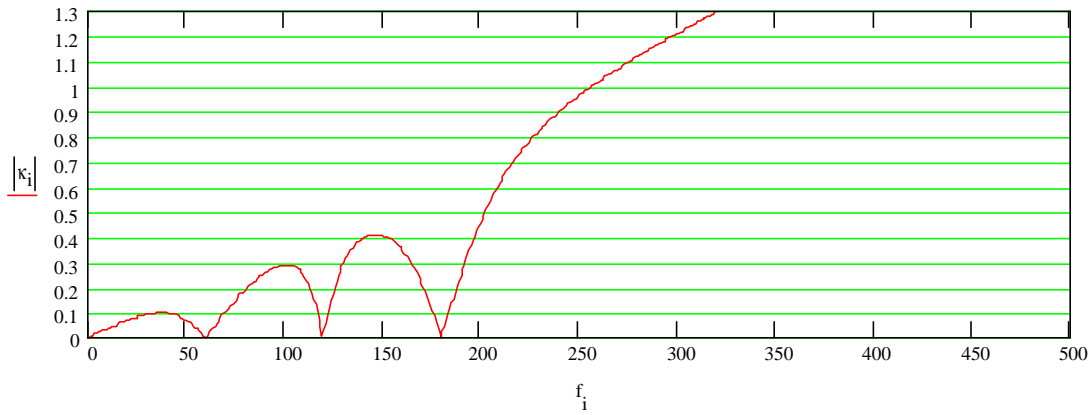
$$K(\mathbf{w}) = \frac{e^{i\mathbf{w}T} - 1}{e^{i\mathbf{w}T} - (1 - k_0)} \frac{e^{i\mathbf{w}T} - e^{i\mathbf{w}_0T}}{e^{i\mathbf{w}T} - (1 - k_1)e^{i\mathbf{w}_0T}} \frac{e^{i\mathbf{w}T} - e^{-i\mathbf{w}_0T}}{e^{i\mathbf{w}T} - (1 - k_1)e^{-i\mathbf{w}_0T}} \cdot \frac{e^{i\mathbf{w}T} - e^{2i\mathbf{w}_0T}}{e^{i\mathbf{w}T} - (1 - k_2)e^{2i\mathbf{w}_0T}} \frac{e^{i\mathbf{w}T} - e^{-2i\mathbf{w}_0T}}{e^{i\mathbf{w}T} - (1 - k_2)e^{-2i\mathbf{w}_0T}} \frac{e^{i\mathbf{w}T} - e^{3i\mathbf{w}_0T}}{e^{i\mathbf{w}T} - (1 - k_3)e^{3i\mathbf{w}_0T}} \frac{e^{i\mathbf{w}T} - e^{-3i\mathbf{w}_0T}}{e^{i\mathbf{w}T} - (1 - k_3)e^{-3i\mathbf{w}_0T}} \quad , \quad (22)$$

where \mathbf{w}_0 is the power line frequency, and k_0, k_1, k_2 and k_3 are the gains (fudge factors) for the corresponding harmonics. The plots of this function for sampling rates of 1.8 kHz and 4.8 kHz are shown in Figure 5. The gains were chosen to fulfill the requirements listed in Section 2. They also determine the minimum sampling frequency of 1.8 kHz¹ which allows to get 20 db suppression at frequency of about 30 Hz. It is important to note that an increase of the sampling frequency significantly decrease the effect of noise measurements so that $\sqrt{\overline{y^2} / \overline{\Delta y^2}}$ decreases from 1.45 at 1.8 kHz to 0.615 at 4.8 kHz. Figure 6 shows relative contribution of different frequencies into the output signal of the feedback system.

¹ This does not imply that sampling frequency cannot be smaller than 1.8 kHz. It rather gives an estimate of the sampling frequency which can be smaller for more advanced algorithm.



a)



b)

Figure 5. Dependence of the module of the feedback system transfer function, $|K(\mathbf{w})|$, on frequency;

a) - $1/T = 4.8$ kHz, $k_0 = 0.35$, $k_1 = 0.03$, $k_2 = 0.01$, and $k_3 = 0.03$, $K(\pi/T) = 1.30$,

b) - $1/T = 1.8$ kHz, $k_0 = 1$, $k_1 = 0.09$, $k_2 = 0.04$, and $k_3 = 0.1$, $K(\pi/T) = 2.52$.

Although a higher order digital filter allows one to decrease the sampling frequency to reach 20 db suppression at region 0-70 Hz the one has to pay for this by additional increase of feedback system noise. The transfer function for the second order system which transfer function is square of the transfer function described by Eq.(22) is shown in Figure 7. For sampling frequency of 900 Hz we obtain

$$\sqrt{y^2 / \Delta y^2} = 3.782 \text{ what is 6 times larger than for 4.8 kHz.}$$

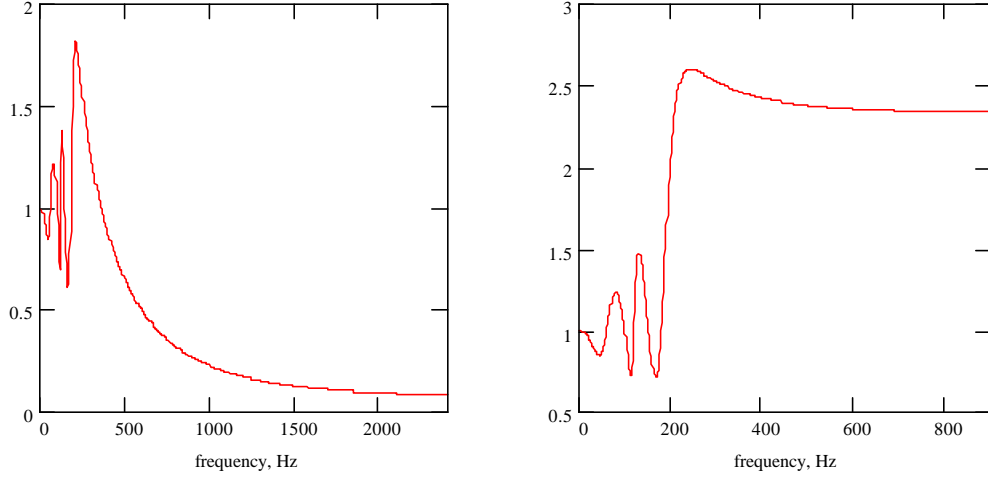


Figure 6. Dependence of relative contribution of measurement noise, $|K(\mathbf{w}) - 1|^2$, on frequency for parameters presented in Figure 5; left - $1/T = 4.8$ kHz, right - $1/T = 1.8$ kHz.

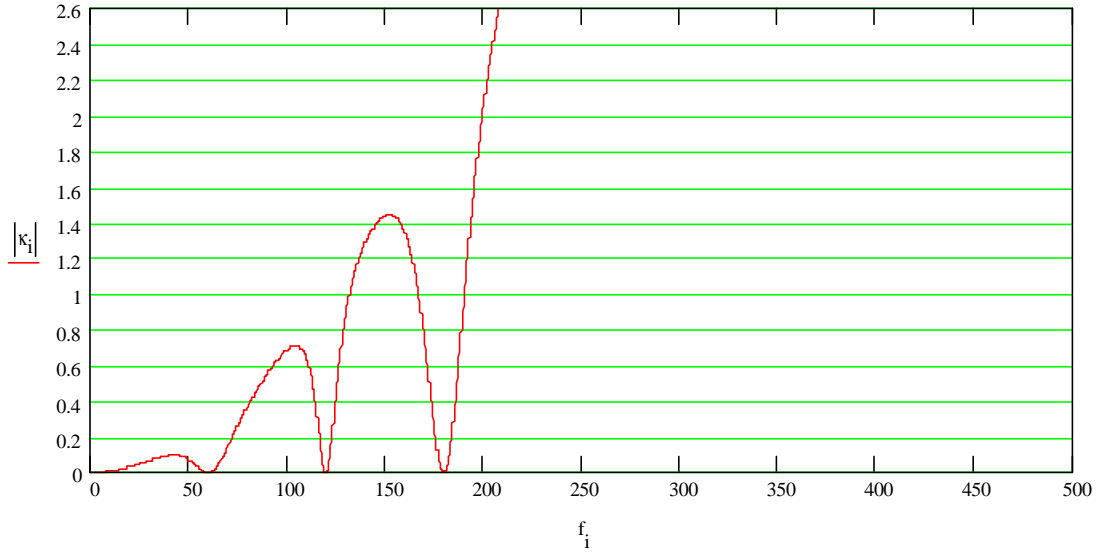


Figure 7. Dependence of the module of the feedback system transfer function, $|K_2(\mathbf{w})| = |K(\mathbf{w})|^2$, on frequency; $1/T = 0.84$ kHz, $k_0 = 1$, $k_1 = 0.1$, $k_2 = 0.05$, and $k_3 = 0.1$, $K(\pi/T) = 6.645$.

To build the numerical algorithm for the filter described by Eq.(22) we will use the standard recipe. Substituting $e^{i\omega T}$ in Eq.(22) by z (rewriting it as the z -transform) and expanding products in the nominator and denominator we obtain

$$K(z) \equiv \frac{y_n}{x_n} = \frac{\sum_{k=0}^7 b_k z^k}{\sum_{k=0}^7 a_k z^k}, \quad (23)$$

where $a_7 = b_7 = 1$ and expressions for other coefficients are given in Appendix. Taking into account that $y_{n+k} = z^k y_n$ and $y_{n+k} = z^k y_n$ we obtain from Eq.(23)

$$\sum_{k=0}^7 a_k y_{n+k} = \sum_{k=0}^7 b_k x_{n+k} \quad , \quad (24)$$

Substituting x_k as $x_k = y_k - c_k$ in Eq.(24) we obtain

$$\sum_{k=0}^7 (a_k - b_k) y_{n+k} + \sum_{k=0}^7 b_k c_{n+k} = 0 \quad . \quad (25)$$

This equation determines correction on each step as weighted sums of previous six corrections and previous six measurements

$$c_{n+1} = \sum_{k=0}^6 (b_k - a_k) y_{n+k-6} - \sum_{k=0}^6 b_k c_{n+k-6} \quad . \quad (26)$$

where we took into account that $a_7 = b_7 = 1$. Figure 8 shows the response of the feedback system to the 60 Hz signal appeared at time $t=0$. The theory predicts that the signal has to be damped for time $t_{\text{damp}} \approx T/k_1 = 7$ ms which is in reasonable coincidence with the results exhibited in Figure 8. Note that the initial fast change is due to the strong damping at zero frequency ($k_0=0.35$).

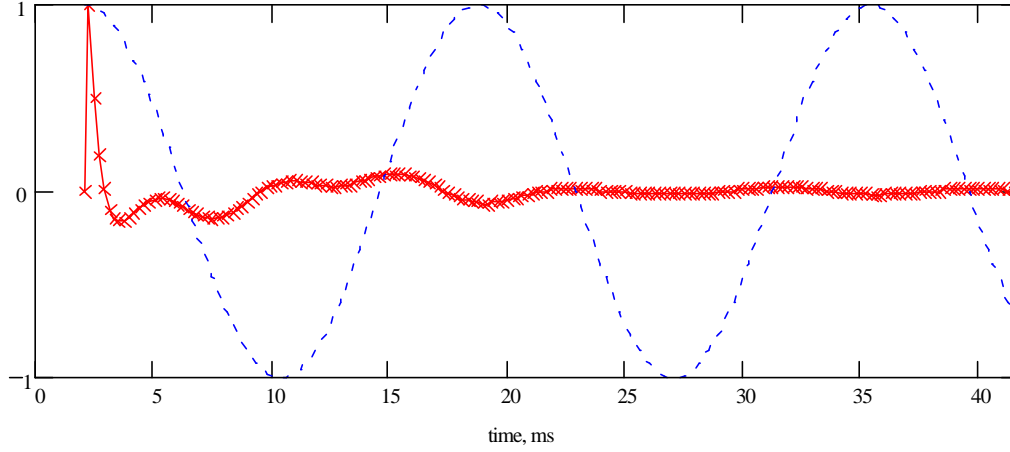


Figure 8. Time response of the feedback system described by Eq.(26) to the 60 Hz signal: dotted line - input signal, solid line - output signal; $1/T = 4.8$ kHz, $k_0 = 0.35$, $k_1 = 0.03$, $k_2 = 0.01$, and $k_3 = 0.03$, $K(\pi/T) = 1.30$,

4. Frequency response and stability of a real feedback system

Now we can consider how the real system operates. In this case values shown in Figure 4 become vectors. Let \vec{x} and \vec{y} and \vec{c} be vectors representing the beam states on the system input and output, so that

$$\vec{x} = \begin{pmatrix} x(t) \\ x'(t) \\ y(t) \\ y'(t) \\ \Delta p(t) / p \end{pmatrix} \quad , \quad (27)$$

and \vec{c} is vector of corrections. The same as in Eq.(11) we can write that

$$\vec{y} = \vec{x} + \vec{c} \quad . \quad (28)$$

Taking into account our limited knowledge of the system we introduce vector \tilde{y}_n representing the estimate of the system state based on BPM measurements \tilde{Y}_n at step n ,

$$\tilde{Y}_n = \mathbf{M} \tilde{y}_n + \Delta \tilde{Y}_n, \quad (29)$$

where \mathbf{M} is the design matrix which relates the BPM measurements and the system state, and $\Delta \tilde{Y}_n$ is the BPM noise. We also introduce the matrix which relates the system state and the actual beam displacements on BPMs

$$\tilde{Y}_n = \tilde{\mathbf{M}} \tilde{y}_n, \quad (30)$$

Then using Eqs.(29) and (30) we can write

$$\tilde{y}_n = \mathbf{M}^{-1} (\tilde{\mathbf{M}} \tilde{y}_n - \Delta \tilde{Y}_n), \quad (31)$$

For the ideal system $\mathbf{M}^{-1} \tilde{\mathbf{M}} = \mathbf{E}$ and Eq.(31) relates \tilde{y} and \tilde{y} within accuracy of the BPM measurements. Our knowledge of the correction system is limited as well. Therefore we introduce the vector of estimated correction (calculated by computer), \tilde{c}_n , which is related to the actual correction by the following equation

$$\bar{c}_n = \mathbf{B} \tilde{c}_n. \quad (32)$$

Then for the case of actual system we can rewrite Eq.(26) as

$$\tilde{c}_{n+1} = \sum_{k=0}^6 (b_k - a_k) \tilde{y}_{n+k-6} - \sum_{k=0}^6 b_k \tilde{c}_{n+k-6}, \quad (33)$$

which represents the algorithm of the feedback system. Substituting Eqs.(31) and (32) we obtain

$$\mathbf{B}^{-1} \bar{c}_{n+1} = \sum_{k=0}^6 (b_k - a_k) (\mathbf{M}^{-1} \tilde{\mathbf{M}} \tilde{y}_{n+k-6} - \mathbf{M}^{-1} \Delta \tilde{Y}_{n+k-6}) - \sum_{k=0}^6 b_k \mathbf{B}^{-1} \bar{c}_{n+k-6}. \quad (34)$$

Multiplying this equation by \mathbf{B} and using Eq.(28) we obtain the equation which relates the input and output system states

$$\tilde{y}_{n+1} - \bar{x}_{n+1} = \sum_{k=0}^6 (b_k - a_k) \mathbf{B} (\mathbf{M}^{-1} \tilde{\mathbf{M}} \tilde{y}_{n+k-6} - \mathbf{M}^{-1} \Delta \tilde{Y}_{n+k-6}) - \sum_{k=0}^6 b_k (\tilde{y}_{n+k-6} - \bar{x}_{n+k-6}). \quad (35)$$

Regrouping addends we finally obtain

$$\tilde{y}_{n+1} - \bar{x}_{n+1} = \sum_{k=0}^6 \left[\left((b_k - a_k) \mathbf{B} \mathbf{M}^{-1} \tilde{\mathbf{M}} - b_k \right) \tilde{y}_{n+k-6} - (b_k - a_k) \mathbf{B} \mathbf{M}^{-1} \Delta \tilde{Y}_{n+k-6} + b_k \bar{x}_{n+k-6} \right]. \quad (36)$$

For the case of the ideal system, $\mathbf{B} \mathbf{M}^{-1} \tilde{\mathbf{M}} = \mathbf{E}$, and zero noise all degrees of freedom in Eq(36) are decoupled and we obtain five scalar equations which are similar to Eq.(24).

To find the transfer function of the system we put

$$\begin{aligned} \bar{x}_n &= \bar{x}_w e^{i\omega n} \\ \tilde{y}_n &= \tilde{y}_w e^{i\omega n} \end{aligned} \quad (37)$$

Then we obtain the transfer function for a real system

$$\begin{aligned} \tilde{y}_w &= \mathbf{K} \bar{x}_w \\ \mathbf{K} &= \left(e^{7i\omega T} + \sum_{k=0}^6 b_k e^{i\omega T k} \right) \left(e^{7i\omega T} \mathbf{E} - \sum_{k=0}^6 \left((b_k - a_k) \mathbf{B} \mathbf{M}^{-1} \tilde{\mathbf{M}} - b_k \mathbf{E} \right) e^{i\omega T k} \right)^{-1}. \end{aligned} \quad (38)$$

The first term in the brackets is equal to the denominator in Eq.(23) and, consequently, has the same zeros. It means that the feedback system will perfectly suppress the signal at desired frequencies even for the case when the transfer matrices are known with finite accuracy. The transfer function at other

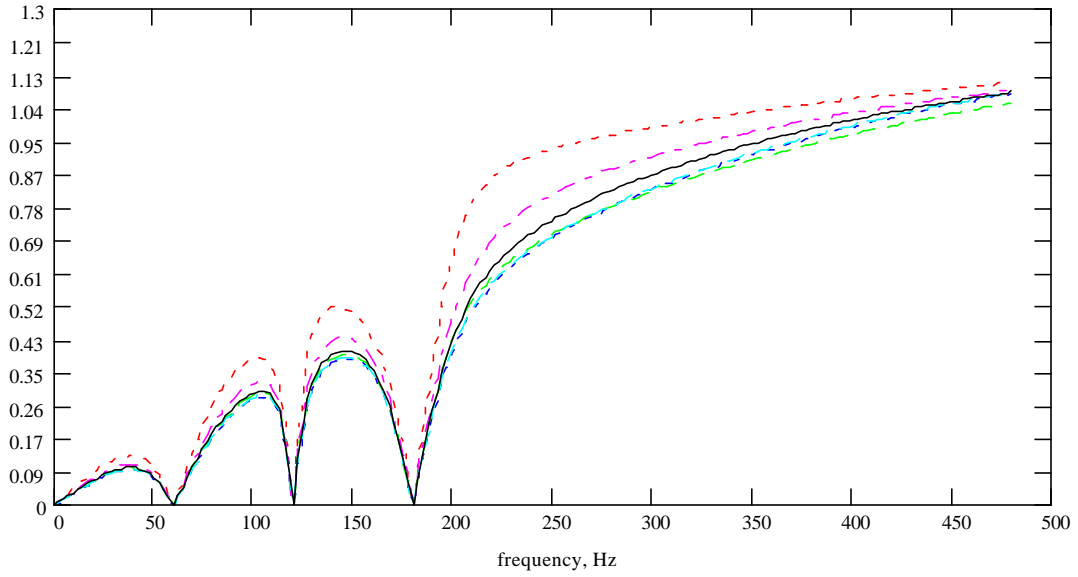
frequencies will be affected by the system nonideality. The Figure 9 shows an example of the system time response to the 60 Hz signal. The product $\mathbf{BM}^{-1}\tilde{\mathbf{M}}$ for this figure was modeled as

$$\mathbf{BM}^{-1}\tilde{\mathbf{M}} = \mathbf{E} + \mathbf{R} \quad , \quad (39)$$

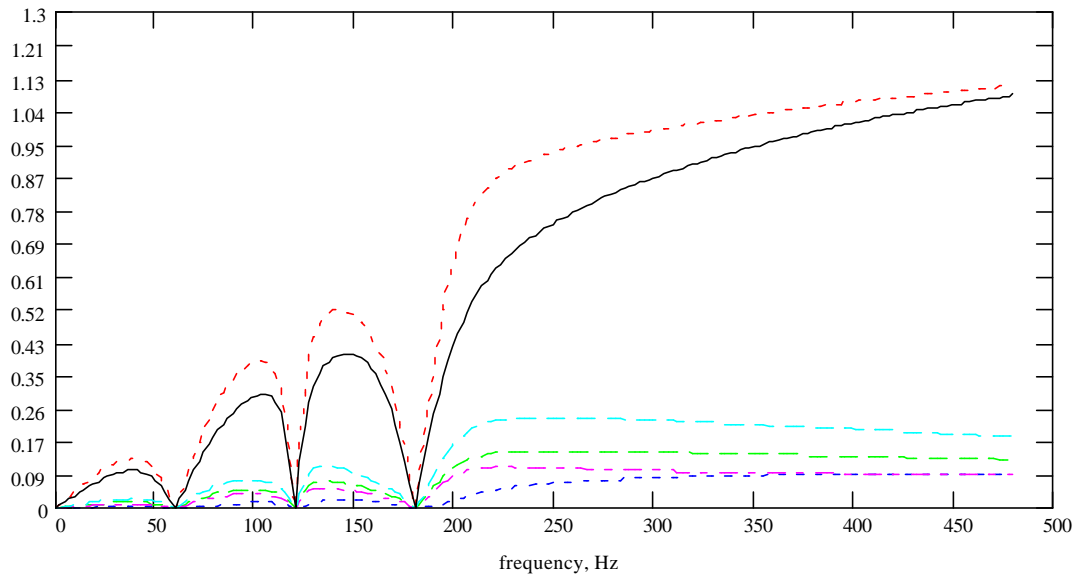
where \mathbf{E} is the unit matrix, and \mathbf{R} is the matrix which elements are random numbers with the uniform distribution in the interval $[-.025, +0.25]$. Numerical simulations for different series of random numbers showed that the picture in Figure 9 represents a typical behavior of the transfer function and we can conclude that the deviation of the transfer function from the design is about relative error of the transfer matrix. It determines that the required accuracy of the transfer matrix knowledge is about 10-20%. Note that for higher value of the system gain the requirements will be harder.

Another important technical limitation which affects the system performance is the accuracy of the sampling time. The interference of sampling errors and the high frequency signal produces additional noise on the system output. The numerical simulation exhibits that a jitter in a sampling time of 30 μs produces the noise from the signal of the third power line harmonic with amplitude of about 3% of the harmonic amplitude, That determines that the sampling accuracy has to be better than 30 μs .

An estimate of the system susceptibility to the BPM noise we will perform for the ideal system. In this case as it was pointed out at the end of Section 2 the energy and position resolution of a single measurement is $\overline{\mathbf{e}_x} = 0.017 \text{ nm}$ and $\sqrt{\Delta p^2} / p = 5.9 \cdot 10^{-6}$ for $x_{BPM} = 20 \mu\text{m}$. Taking into account that for the feedback system considered above the real beam displacement is smaller than its estimate in a factor of 0.615 (see Section 3) we finally obtain $\overline{\mathbf{e}_x} = 0.007 \text{ nm}$ and $\sqrt{\Delta p^2} / p = 3.6 \cdot 10^{-6}$. This values will not be changed significantly if the machine optics is known with 5-10% accuracy.



a)



b)

Figure 9. Frequency response, $\mathbf{K}(f)$, for non-ideal feedback system. a) solid line - response for the ideal system, other lines - \mathbf{K}_{11} , \mathbf{K}_{22} , \mathbf{K}_{33} , \mathbf{K}_{44} and \mathbf{K}_{55} ; b) solid line - response for the ideal system, top dotted line - \mathbf{K}_{11} , other lines - \mathbf{K}_{12} , \mathbf{K}_{13} , \mathbf{K}_{14} and \mathbf{K}_{15} .

Appendix. Formulas for calculation of the digital filter coefficients.

$$\Lambda r_1 := \operatorname{Re}(\Lambda_1)$$

$$\Lambda r_2 := \operatorname{Re}(\Lambda_2)$$

$$\Lambda r_3 := \operatorname{Re}(\Lambda_3)$$

$$\text{Nom} = (\lambda - 1) \cdot (\lambda^2 - 2\Lambda r_1 \lambda + 1) \cdot (\lambda^2 - 2\Lambda r_2 \lambda + 1) \cdot (\lambda^2 - 2\Lambda r_3 \lambda + 1)$$

$$b := \begin{bmatrix} -1 \\ 2\Lambda r_1 + 1 + 2\Lambda r_2 + 2\Lambda r_3 \\ -2\Lambda r_3 - 3 - 4\Lambda r_1 \Lambda r_2 - 4\Lambda r_2 \Lambda r_3 - 2\Lambda r_1 - 2\Lambda r_2 - 4\Lambda r_1 \Lambda r_3 \\ 4\Lambda r_3 + 4\Lambda r_1 \Lambda r_3 + 3 + 4\Lambda r_1 \Lambda r_2 + 4\Lambda r_2 \Lambda r_3 + 4\Lambda r_2 + 4\Lambda r_1 + 8\Lambda r_1 \Lambda r_2 \Lambda r_3 \\ -3 - 4\Lambda r_3 - 8\Lambda r_1 \Lambda r_2 \Lambda r_3 - 4\Lambda r_2 \Lambda r_3 - 4\Lambda r_1 \Lambda r_3 - 4\Lambda r_1 \Lambda r_2 - 4\Lambda r_2 - 4\Lambda r_1 \\ 2\Lambda r_2 + 2\Lambda r_1 + 3 + 4\Lambda r_1 \Lambda r_2 + 4\Lambda r_2 \Lambda r_3 + 4\Lambda r_1 \Lambda r_3 + 2\Lambda r_3 \\ -1 - 2\Lambda r_3 - 2\Lambda r_1 - 2\Lambda r_2 \\ 1 \end{bmatrix}$$

$$q_0 := 1 - k_0$$

$$q_1 := 1 - k_1$$

$$q_2 := 1 - k_2$$

$$q_3 := 1 - k_3$$

$$\Lambda k_1 := q_1 \cdot \operatorname{Re}(\Lambda_1)$$

$$\Lambda k_2 := q_2 \cdot \operatorname{Re}(\Lambda_2)$$

$$\Lambda k_3 := q_3 \cdot \operatorname{Re}(\Lambda_3)$$

$$\text{Denom} = (\lambda - q_0) \cdot (\lambda^2 - 2\Lambda k_1 \lambda + q_1^2) \cdot (\lambda^2 - 2\Lambda k_2 \lambda + q_2^2) \cdot (\lambda^2 - 2\Lambda k_3 \lambda + q_3^2)$$

$$D_0 := q_2^2 \cdot q_3^2 + 2q_0 \Lambda k_2 q_3^2 + 2q_0 \Lambda k_1 q_3^2 + 2q_0 q_2^2 \Lambda k_3 + 8q_0 \Lambda k_1 \Lambda k_2 \Lambda k_3 + 2q_0 \Lambda k_1 q_2^2 + 2q_0 q_1^2 \Lambda k_3$$

$$D_1 := D_0 + 2q_0 q_1^2 \Lambda k_2 + 4q_1^2 \Lambda k_2 \Lambda k_3 + 4\Lambda k_1 q_2^2 \Lambda k_3 + q_1^2 q_3^2 + 4\Lambda k_1 \Lambda k_2 q_3^2 + q_1^2 q_2^2$$

$$\begin{aligned}
& -q_0 q_1^2 q_2^2 q_3^2 \\
& q_1^2 q_2^2 q_3^2 + 2q_0 \Lambda k_1 q_2^2 q_3^2 + 2q_0 q_1^2 \Lambda k_2 q_3^2 + 2q_0 q_1^2 q_2^2 \Lambda k_3 \\
& -q_0 q_1^2 q_2^2 - 4q_0 \Lambda k_1 \Lambda k_2 q_3^2 - q_0 q_2^2 q_3^2 - 4q_0 \Lambda k_1 q_2^2 \Lambda k_3 - 2\Lambda k_1 q_2^2 q_3^2 - 2q_1^2 q_2^2 \Lambda k_3 - 2q_1^2 \Lambda k_2 q_3^2 - 4q_0 q_1^2 \Lambda k_2 \Lambda k_3 - q_0 q_1^2 q_3^2 \\
a := & q_2^2 q_3^2 + 2q_0 \Lambda k_2 q_3^2 + 2q_0 \Lambda k_1 q_3^2 + 2q_0 q_2^2 \Lambda k_3 + 8q_0 \Lambda k_1 \Lambda k_2 \Lambda k_3 + 2q_0 \Lambda k_1 q_2^2 + 2q_0 q_1^2 \Lambda k_3 + 2q_0 q_1^2 \Lambda k_2 + 4q_1^2 \Lambda k_2 \Lambda k_3 + 4\Lambda k_1 q_2^2 \Lambda k_3 + q_1^2 q_3^2 + 4\Lambda k_1 \Lambda k_2 q_3^2 + q_1^2 q_2^2 \\
& -2\Lambda k_2 q_3^2 - 2q_2^2 \Lambda k_3 - 8\Lambda k_1 \Lambda k_2 \Lambda k_3 - 4q_0 \Lambda k_2 \Lambda k_3 - q_0 q_3^2 - 4q_0 \Lambda k_1 \Lambda k_3 - q_0 q_2^2 - 4q_0 \Lambda k_1 \Lambda k_2 - q_0 q_1^2 - 2q_1^2 \Lambda k_3 - 2\Lambda k_1 q_3^2 - 2\Lambda k_1 q_2^2 - 2q_1^2 \Lambda k_2 \\
& 4\Lambda k_2 \Lambda k_3 + 4\Lambda k_1 \Lambda k_3 + q_1^2 + 2q_0 \Lambda k_1 + 2q_0 \Lambda k_2 + 2q_0 \Lambda k_3 + q_2^2 + q_3^2 + 4\Lambda k_1 \Lambda k_2 \\
& -q_0 - 2\Lambda k_1 - 2\Lambda k_2 - 2\Lambda k_3 \\
& 1
\end{aligned}$$